Supplementary Materials for

Key Role of Meniscus Shape on Crystallization of Organic Semiconductors during Meniscus-Guided Coating

Ke Zhang,[1] Zuyuan Wang,[1] Tomasz Marszalek,[1,2] Michal Borkowski,[2] Georg Fytas,[1] Paul W. M. Blom,[1] Wojciech Pisula*[,1,2]

[1] Max Planck Institute for Polymer Research, Ackermannweg 10, 55128 Mainz, Germany
[2] Department of Molecular Physics, Faculty of Chemistry, Lodz University of Technology, Zeromskiego 116, 90-924 Lodz, Poland

*To whom correspondence should be addressed.
Email: pisula@mpip-mainz.mpg.de

Contents:

1. ADDC of C8-BTBT

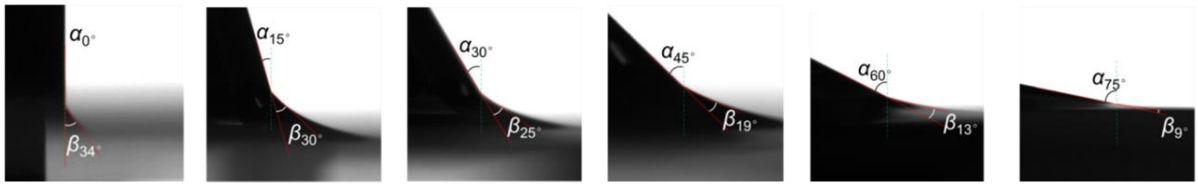

Fig. S1. Illustration and meniscus shape of ADDC at different tilt angles. The meniscus shape on the silicon substrate (treated by oxygen plasma, S_{plasma}) in $CHCl_3$ at different tilt angles. The meniscus shape is described by the meniscus angle (β).

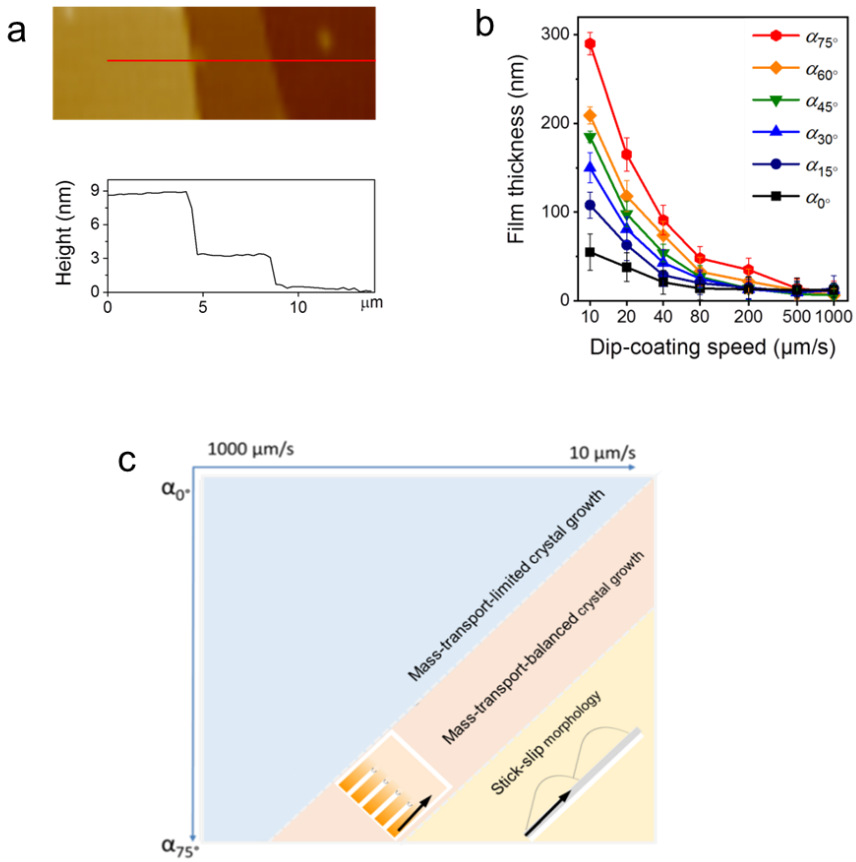

Fig. S2. ADDC of C8-BTBT and film growth regime. (a) Height plot of dip-coated C8-BTBT at 20 µm/s to determine the interlayer thickness (analogous to Fig. 1e). (b) Film thickness of C8-BTBT for different α as a function of dip-coating speed. (c) Subdivision of different growth regimes during ADDC of C8-BTBT (compare to Fig. 2).

2. Evaporation rate of bulk solution during ADDC

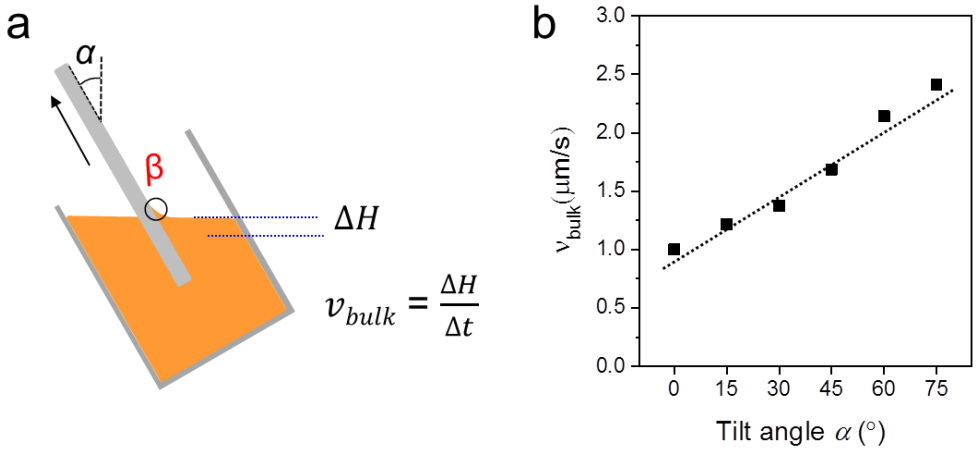

Fig. S3. Evaporation rate of bulk solution during ADDC. (a) Average evaporation rates for bulk solution (v_{bulk}) for different α determined by the decrease of the liquid level of the bulk solution in container per second. (b) Relation between v_{bulk} and α.

During ADDC of C8-BTBT, the tilt of container changes the liquid level of solution and varies in this way the solvent evaporation rates (v_{bulk}). To perform fluid simulation, average $v_{bulk(\alpha)}$ for different α are estimated by

$$v_{bulk} = \frac{\Delta H}{\Delta t} \tag{1}$$

wherein Δ is the decreased height of liquid level during the time of (Δt) (Fig. S3a). The average $v_{bulk(\alpha)}$ are shown in Figure S3b.

During dip-coating, the deposited film thickness is proportional to the solvent evaporation rate v_{bulk}

$$h = k_i \times \frac{v_{bulk}}{v_{\text{coating}}} \tag{2}$$

Therefore, the influence of varied $v_{bulk(\alpha)}$ on film thickness was estimated by the following equation (3)

$$h_{(\alpha)} = h_{(0°)} \times \frac{v_{bulk(\alpha)}}{v_{bulk(0°)}} \tag{3}$$

wherein $h_{(\alpha)}$ is the film thickness at α, $h_{(0°)}$ is the film thickness at α=0°, $v_{bulk(\alpha)}$ and $v_{bulk(0°)}$ are the bulk evaporation rate at α and 0°, respectively. (*1*) As shown in Fig. S3b, the estimated film thickness ($h_{(\alpha)}$) based on varied $v_{bulk(\alpha)}$ and $h_{(0°)}$ is indicated by blue dots.

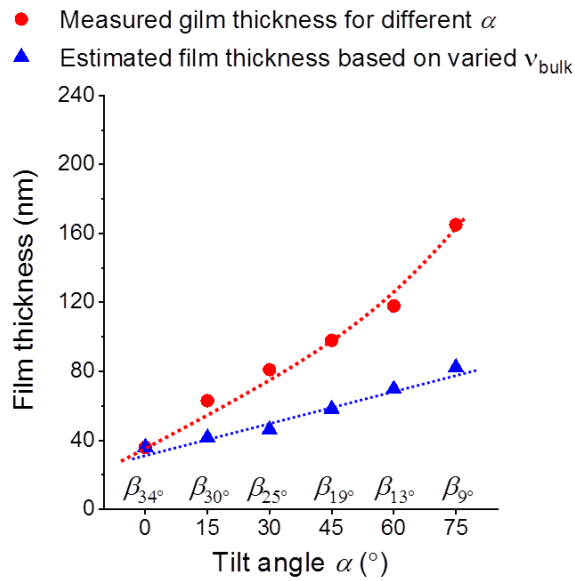

Fig. S4. Measured film thickness of C8-BTBT obtained by ADDC at 20 μm/s is indicated by red dots. Dashed lines are eye guides. The effect of varied v_{bulk} on dip-coating thickness is estimated from equation (3) (blue dots).

3. Two-dimensional fluid simulation of ADDC

The governing equations are the steady state, two-dimensional continuity equation, momentum transport equation, and mass transport equation. Because of the small Reynolds numbers (Re < 1), the flow involved during dip-coating can be considered as Stokes flow (or creeping flow). For Stokes flow (or creeping flow), gravity has a negligible effect on the momentum and mass transport. (*2*) As a result, the simulation domains can be rotated around point O clockwise by the tilt angle (α) so that the domain becomes vertically oriented (see Fig. S5). This rotation significantly simplifies the expressions of the boundary conditions. After determining the governing equations, we derived the boundary conditions that are appropriate for the dip-coating simulations. There are five boundaries: (1) B1: segment TP; (2) B2: segment PQ; (3) B3: segment QR; (4) B4: segment RO + elliptic arc OS; (5) B5: segment TS (truncated boundary to avoid the singularity problem in generating meshes). The corresponding physics models in COMSOL are the transport of dilute species model and the creeping flow model. For all the six simulations (i.e., α = 0°, 15°, 30°, 45°, 60°, 75°), we adopt the following parameters: dip-coating speed at 20 μm/s, solute concentration of bulk solution, c_{bulk} = 0.003 g/mL.

The evaporation rate at the meniscus (v_m) for different α is determined by the solvent vapor pressure, which is related to meniscus height (Fig. 3b) and $v_{bulk(\alpha)}$. The results calculated by the fluid simulation are shown in Figs. 3c.

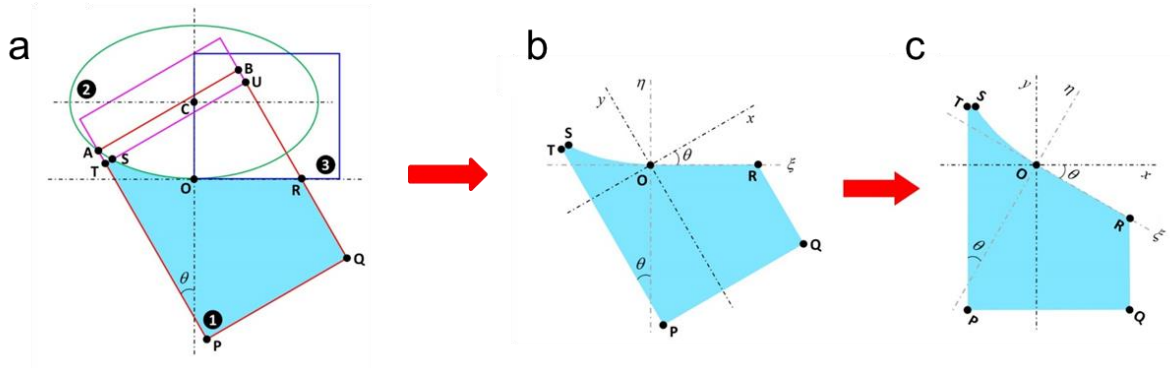

Fig. S5. Two-dimensional fluid simulation. (a) Schematic illustration of a simulation domain. To simply the expressions of the boundary conditions, (b) the simulation domain was rotated clockwise by the tilt angle α to obtain (c) the simplified simulation domain. The rotation axis is normal to the page and passes through point O.

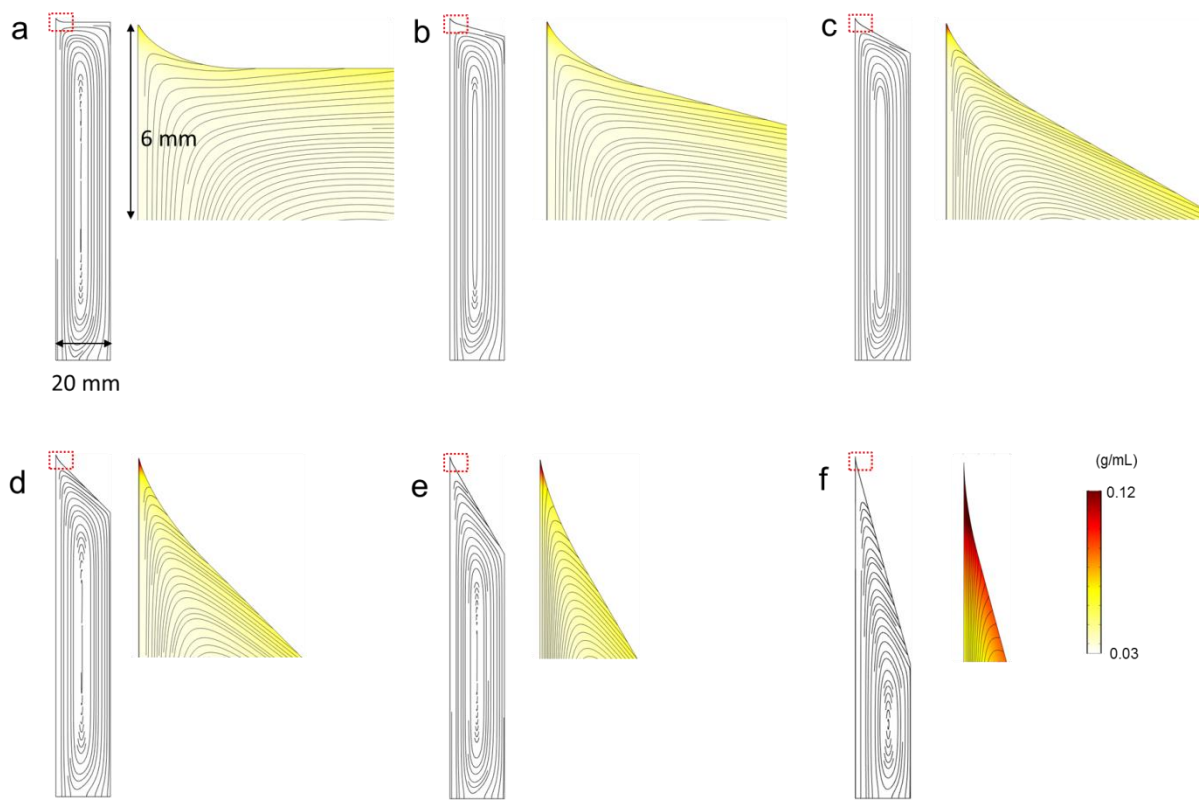

Fig. S6. Calculated concentration distributions and streamline based on $v_{bulk(0°)}$. Concentration and streamline at (a) $\alpha_{0°}$, (b) $\alpha_{15°}$, (c) $\alpha_{30°}$, (d) $\alpha_{45°}$, (e) $\alpha_{60°}$, (f) $\alpha_{75°}$. The width of the entire simulated regime is 25 mm and the height of selected area is 6 mm.

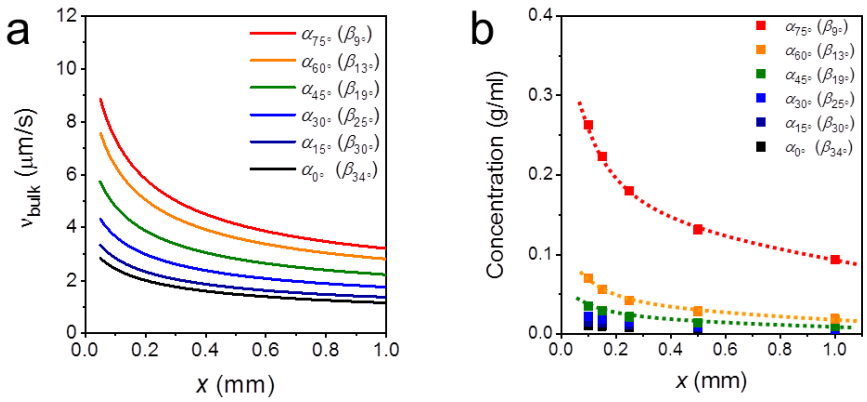

Fig. S7 Two-dimensional fluid simulation for ADDC based on $v_{bulk}(\alpha)$. (a) Evaporation rate at the meniscus (v_m) as a function of x. (b) Calculated solute concentration at the meniscus (c_m) as a function of x.

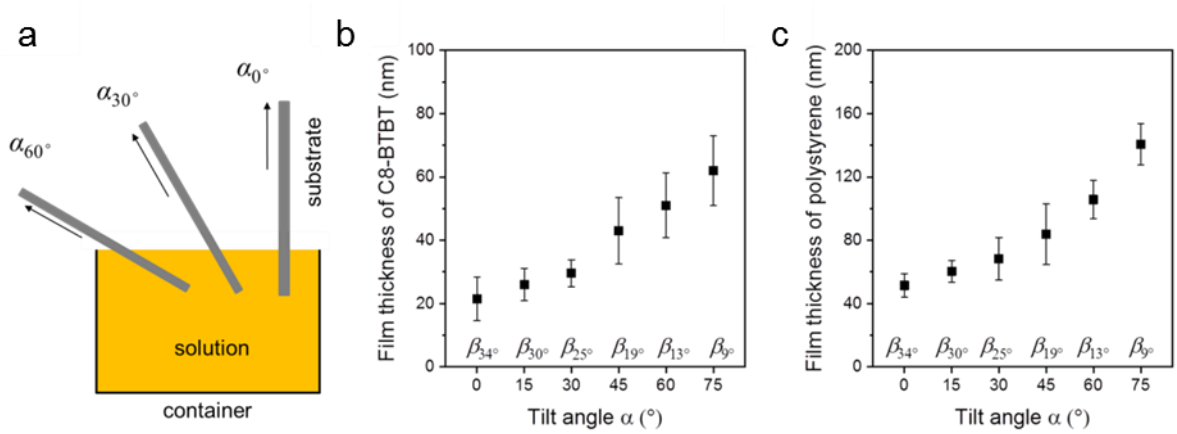

Fig. S8. ADDC from large container. (a) Schematic illustration of ADDC from large container (50 mL) completely filled by the solution achieving a constant v_{bulk} at experimental conditions. (b) Film thickness of C8-BTBT obtained by ADDC at 200 μm/s from large container completely filled by $CHCl_3$ (3 mg/mL). (c) Film thickness of polystyrene (400 kDa) obtained by ADDC at 80 μm/s from large container completely filled by $CHCl_3$ (1 mg/mL).

4. Fluid flow assisted crystallization on substrates with different surface energy

Determination of surface energy of substrate via the equation of state approach (*3*):

$$\cos\theta = -1 + 2\sqrt{\frac{\gamma_{SV}}{\gamma_{LV}}}(1 - \xi(\gamma_{LV} - \gamma_{SV})^2) \quad (2)$$

wherein γ_{LV} is the surface tension of solvent and γ_{SV} is the substrate surface energy, and ξ is an empirical constant unique for each substrate, introduced to reduce the fitting error.

Table S1. Contact angle of probe liquids on various substrates.

Solvent	γ_{LV} (mN/m)	S_{OTS}	S_{HMDS}	S_{bare}	S_{plasma}
Ethylene glycol	47.7	104.2±3.4	87.2±2.9	46.0±4.3	11.2±1.9
Formamide	59.1	96.6±1.3	81.1±1.5	40.2±2.5	11.0±1.3
Glycerol	65.0	92.0±1.3	67.0±2.7	29.3±2.2	
Water	72.7	68.4±2.6	30.3±2.0		

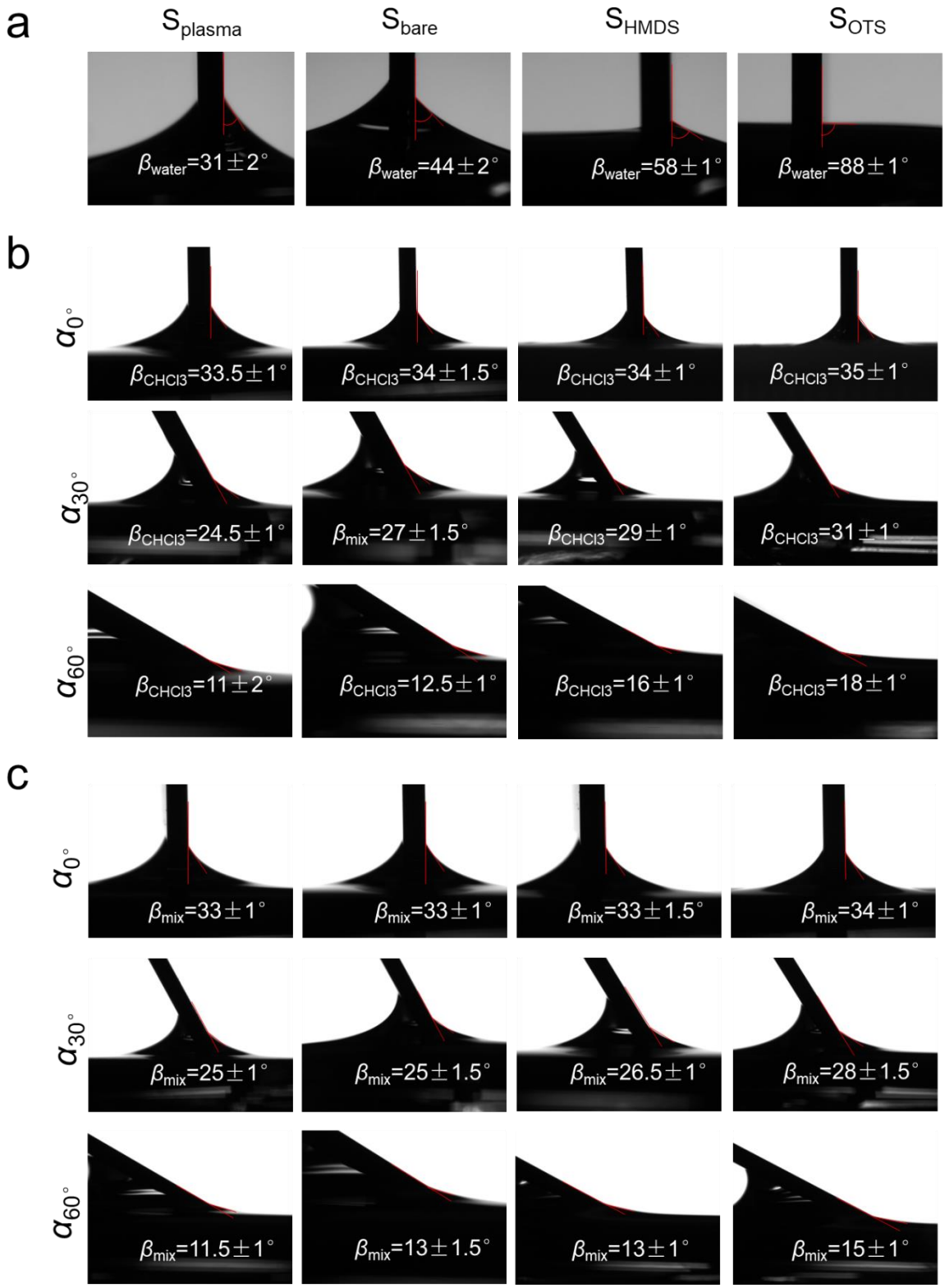

Fig. S9. Optical microscopy images of meniscus angle. (a) Meniscus angles of water (β_{water}) at substrates with different surface energy for $\alpha_{0°}$. (b) Meniscus angles of $CHCl_3$ (β_{CHCl3}) at substrates with different surface energy for $\alpha_{0°}$, $\alpha_{30°}$ and $\alpha_{60°}$. (c) Meniscus angles of mixed-solvent (β_{mix}) at substrates with different surface energy for $\alpha_{0°}$, $\alpha_{30°}$ and $\alpha_{60°}$.

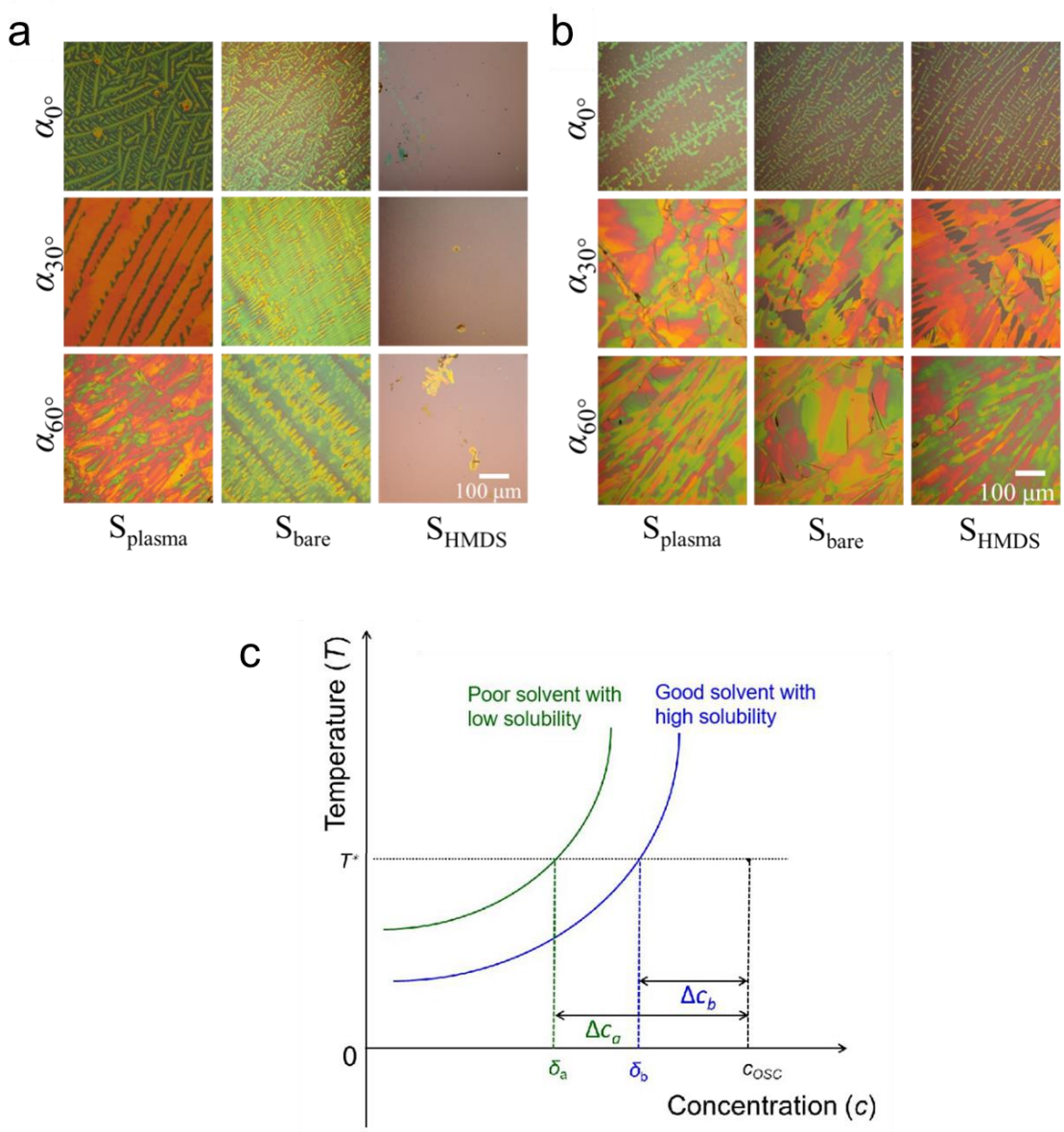

Fig. S10. Influence of solvent on OSC crystallization. Optical microscopy images of C8-BTBT obtained at 20 µm/s and at $\alpha_{0°}$, $\alpha_{30°}$ and $\alpha_{60°}$ on substrates with different surface energy from (a) $CHCl_3$ and (b) mixed-solvent (4:1 $CHCl_3$:hexane). Scale bar is valid for all images. (c). The influence of solubility on concentration supersaturation. At T*, the supersaturation for OSC in good solvent is Δc_b ($\Delta c_b = c_{OSC} - \delta_b$) and in poor solvent is Δc_a ($\Delta c_a = c_{OSC} - \delta_a$), where $\Delta c_b < \Delta c_a$.

5. **Molecular packing and charge transport characterizations.**

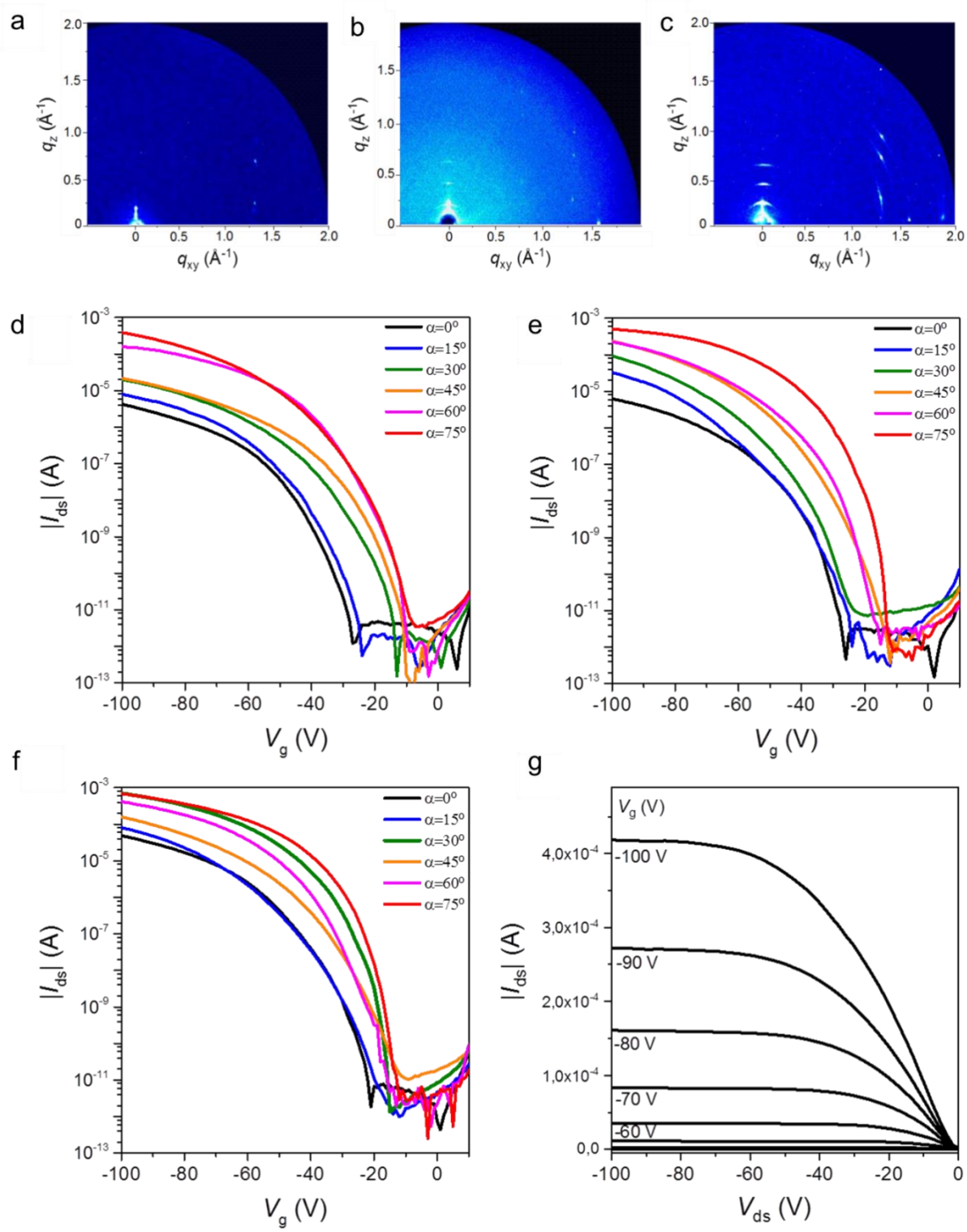

Fig. S11. Molecular packing and charge transport characterizations. GIWAXS patterns of dip-coated C8-BTBT at 20 µm/s from $CHCl_3$ on S_{plasma} for (a) $\alpha_{0°}$, (b) $\alpha_{30°}$ and (c) $\alpha_{60°}$. Transfer curves at V_{ds}= -100 V for C8-BTBT dip-coated on S_{plasma} from 3 mg/mL $CHCl_3$ at (d) 200 µm/s, (e) 80 µm/s, and (f) 20 µm/s. (g) Output curve of C8-BTBT obtained at $\alpha_{75°}$ and 80 µm/s on S_{plasma} from 3 mg/mL $CHCl_3$.

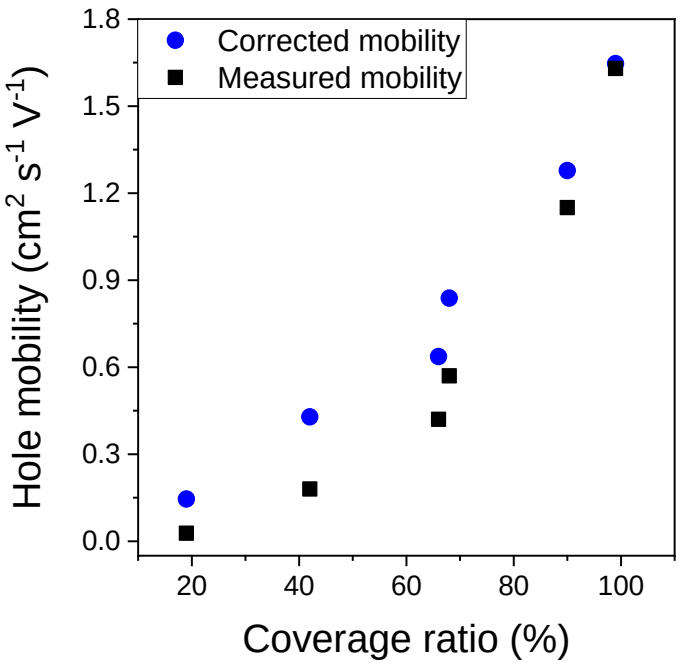

Fig. S12. Relation between corrected hole mobility and coverage ratio for C8-BTBT on S_{plasma} from $CHCl_3$ at 80 μm/s (corresponding to Figure 5c).

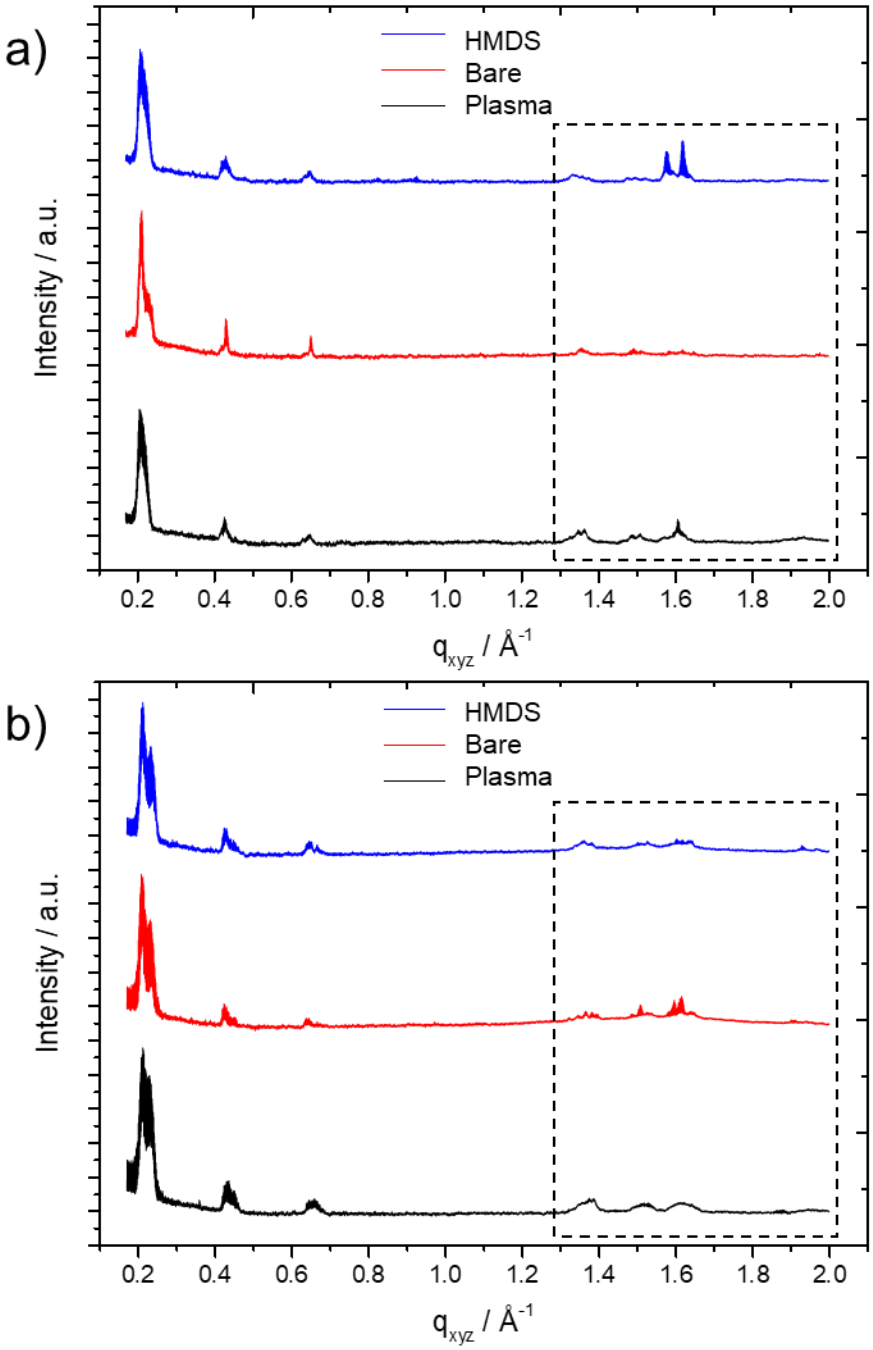

Fig. S13. a) Perpendicular and b) parallel GIWAXS of dip-coated C8-BTBT on different substrates from mixed-solvent at 20 µm/s and $\alpha_{60°}$. The GIWAXS corresponds to the transfer curves in Fig. 5d. The dashed frame indicates peaks related to the in-plane molecular packing.

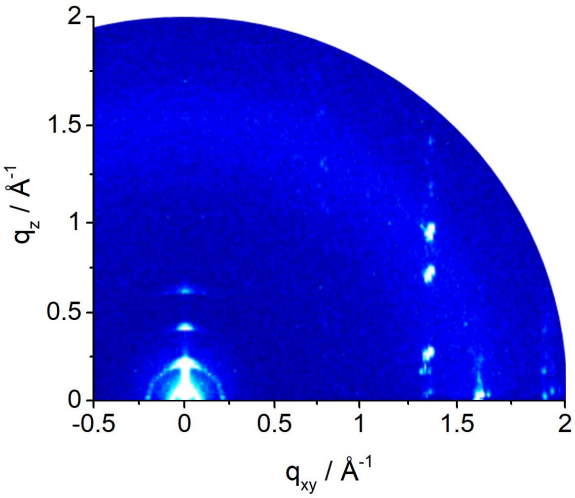

Fig. S14. GIWAXS pattern recorded parallel to the dip-coating direction for C8-BTBT cast from mixed-solvent at 20 μm/s and $\alpha_{60°}$ on bare SiO_2 (corresponds to Figure S13b).

References

1. D. Grosso, How to exploit the full potential of the dip-coating process to better control film formation. *J. Mater. Chem.* **21**, 17033-17038 (2011).
2. C. Hsueh, F. Doumenc, B.Guerrier, Numerical simulation of complex fluid drying in a Hele-Shaw cell, *Europ. Phys. J. Special Topics*, **219**(1), 51-57 (2013).
3. F. Zhang *et al.*, Critical role of surface energy in guiding crystallization of solution-coated conjugated polymer thin films. *Langmuir* **34**, 1109-1122 (2018).